A few thoughts about configuration mixing calculations

- The general framework
- Particle number symmetry
- Approximations to configuration mixing
- Choice of basis and accuracy
- Octupoles: - first applications
  - fission barriers and odd nuclei

BriX

ULB

- Most calculations by W. Ryssens (PhD in ULB and IPNL post doc)
- And by Michael Bender
- V. Hellemans for some octupole applications

Symmetry restoration + configuration mixing on HFB wave functions

(i) First step: vacuum or “false vacuum”

$$|\mathrm{HFB_{fv}}(q_1,q_2)\rangle = \prod_{k>0}(u_k + v_k a_k^\dagger a_{\bar{k}}^\dagger)|-\rangle,$$

Constraint on N and Z but no qp excitation.
Put the Fermi energy at the right place.

(ii) Second step: several 1qp or 2qp states are calculated self-consistently for each (q1,q2) or (q1,q3)

(iii) For each state, restoration of symmetry and K-mixing (or parity)

$$|J^\pi M \kappa(\mu)\rangle = \sum_{K=-J}^{J} f_{\mu,K}^{J^\pi \kappa}\, \hat{P}^J_{MK} \hat{P}^N \hat{P}^Z |\mathrm{HFB}^\pi_{1\mathrm{qp}}(\mu)\rangle$$

The coefficients *f* are determined by the HWG equation:

$$\sum_{K'} \left(\mathcal{H}^{J^\pi}_{\mu,K;\mu,K'} - E^{J^\pi}_\kappa \mathcal{I}^{J^\pi}_{\mu,K;\mu,K'} \right) f^{J^\pi \kappa}_{\mu,K'} = 0$$

It requires to calculate the overlap and Hamiltonian kernels:

$$\mathcal{I}^{J^\pi}_{\mu,K;\mu',K'} \equiv \langle \mathrm{HFB}^\pi_{1\mathrm{qp}}(\mu)|\hat{P}^J_{KK'}\hat{P}^Z\hat{P}^N|\mathrm{HFB}^\pi_{1\mathrm{qp}}(\mu')\rangle$$

$$\mathcal{H}^{J^\pi}_{\mu,K;\mu',K'} \equiv \langle \mathrm{HFB}^\pi_{1\mathrm{qp}}(\mu)|H P^J_{KK'}P^Z P^N|\mathrm{HFB}^\pi_{1\mathrm{qp}}(\mu')\rangle$$

(iiii) Last step: configuration mixing on the quadrupole deformation (q_1 q_2) of all the states projected on (JM, N, Z). Several states for each deformation!

$$|J^\pi M\xi\rangle = \sum_{\mu=1}^{\Omega_I}\sum_{\kappa} f^{J^\pi\xi}_{\mu,\kappa}\,|J^\pi M\kappa(\mu)\rangle$$

At steps 3 and 4, removal of states corresponding to small values of the norm or to non-accurate values of $\langle J^2\rangle$

projection

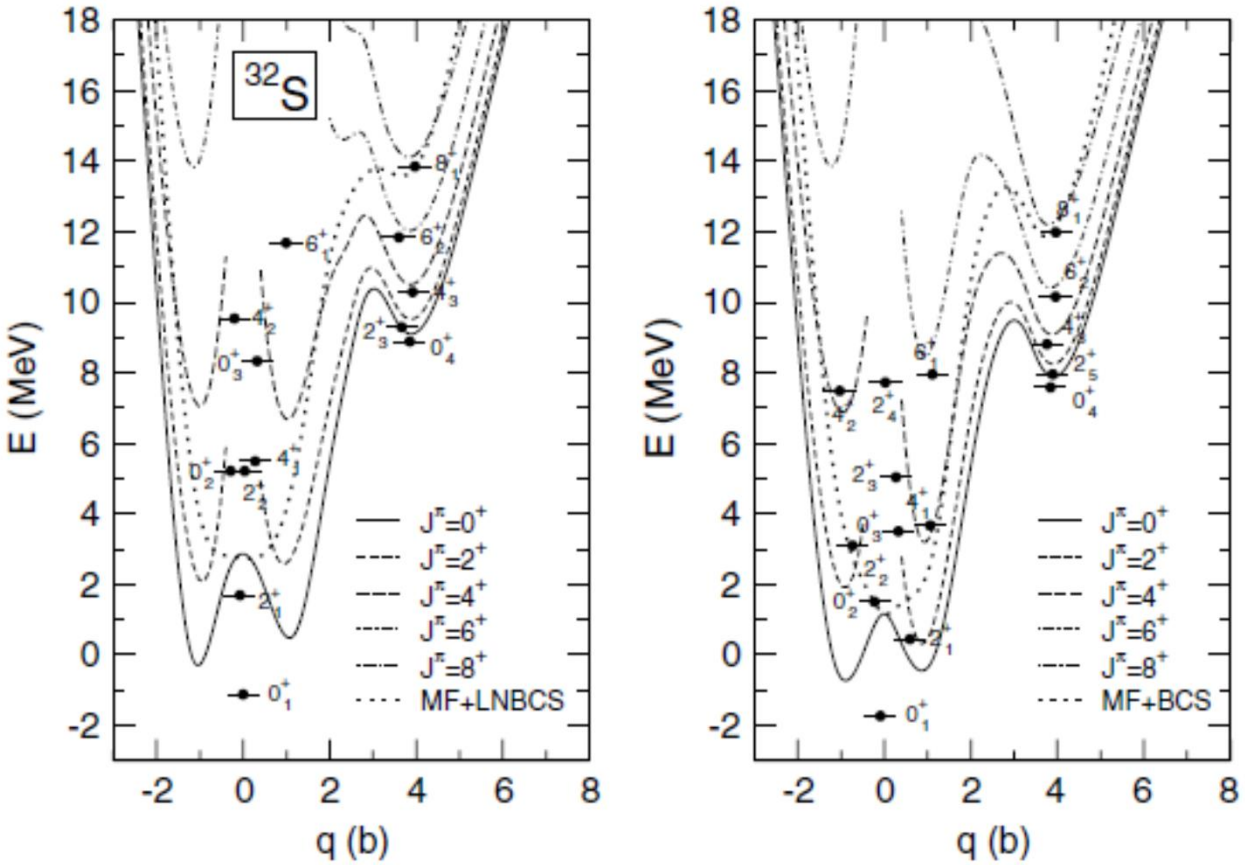

Approximate pn correction

FIG. 6. The energies and the average quadrupole moments of the GCM states in ^{32}S, plotted together with the corresponding angular momentum projected energy curves. GCM calculations with (left panel), and without (right panel) particle number projection are compared. The mean-field binding energy curves are also included in the figure (dotted curves). In both panels zero energy corresponds to the minimum of the $J = 0$ projected energy curve.

PHYSICAL REVIEW C 74, 064309 (2006)

T. Nikšić & D. Vretenar and P. Ring

Non-relativistic EDF calculations without PNP

^{80}Zr: Comparison of spectra

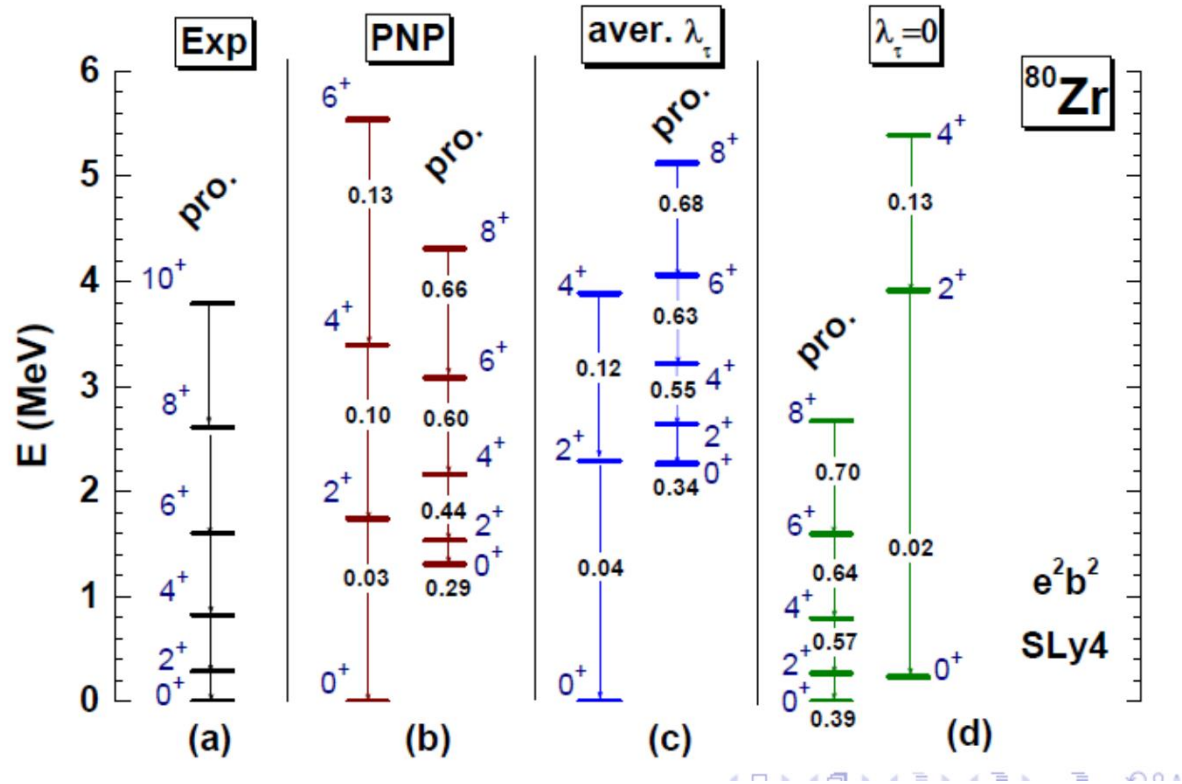

Yao Bender and PHH unpublished

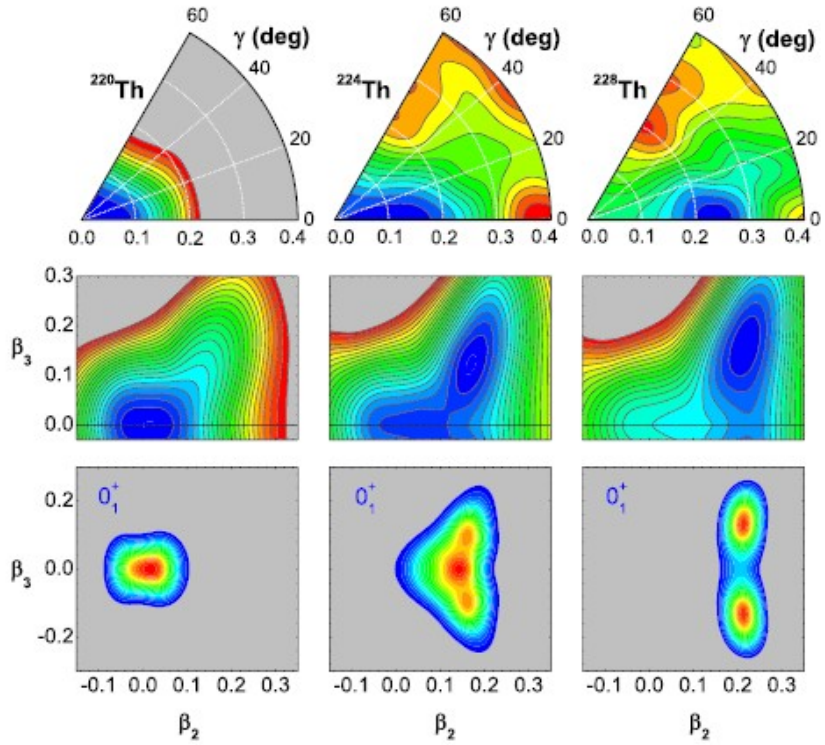

Fig. 1. (Color online.) Self-consistent RMF+BCS triaxial quadrupole energy surfaces in the β_2–γ plane ($0 \leqslant \gamma \leqslant 60°$) (upper panels), and axially-symmetric quadrupole octupole energy surfaces in the β_2–β_3 plane (middle panels), for ^{220,224,228}Th. The contours join points on the surface with the same energy, and the separation betwee neighboring contours is 0.5 MeV. Probability density distributions for the ground states 0_1^+ of ^{220,224,228}Th in the β_2–β_3 plane (lower panels).

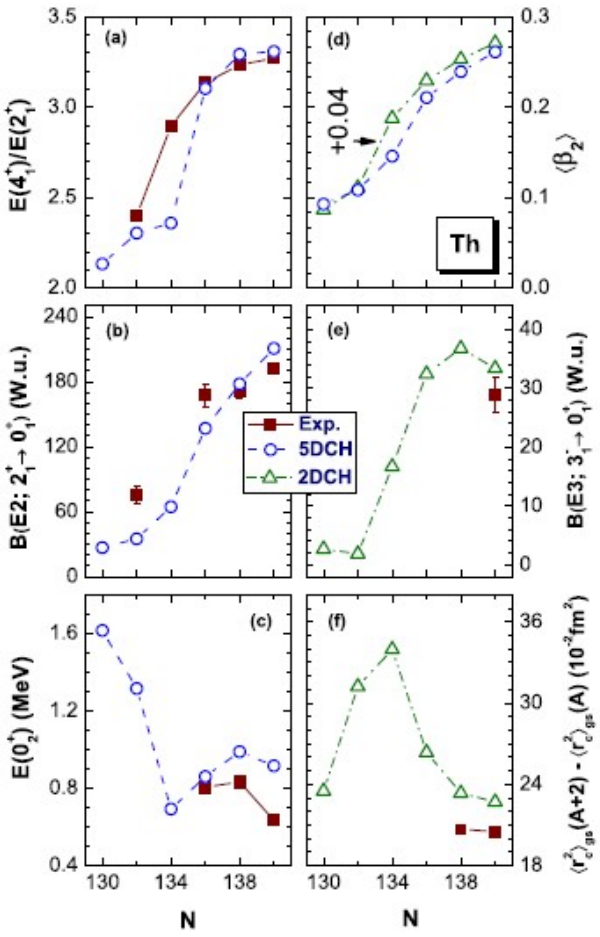

Fig. 2. (Color online.) Evolution of the energy ratios $E(4_1^+)/E(2_1^+)$ (a), $B(E2; 2_1^+ \to 0_1^+)$ values (b), excitation energies of 0_2^+ states (c), expectation values of the quadrupole deformation parameter $\langle\beta_2\rangle$ in the ground state 0_1^+ (d), $B(E3; 3_1^- \to 0_1^+)$ (e), and the isotope shifts of the ground-state charge radii: $\langle r_c^2\rangle_{gs}(A+2) - \langle r_c^2\rangle_{gs}(A)$ (f), as functions of the neutron number in Th isotopes. Microscopic values calculated with the 5D (three-dimensional rotations and β_2–γ quadrupole vibrations) (circles), and 2D (axially-symmetric quadrupole–octupole vibrations) (triangles) collective Hamiltonians based on the PC-PK1 density functional are compared to available data.

5D or 2D collective Hamiltonian based on RMF surface

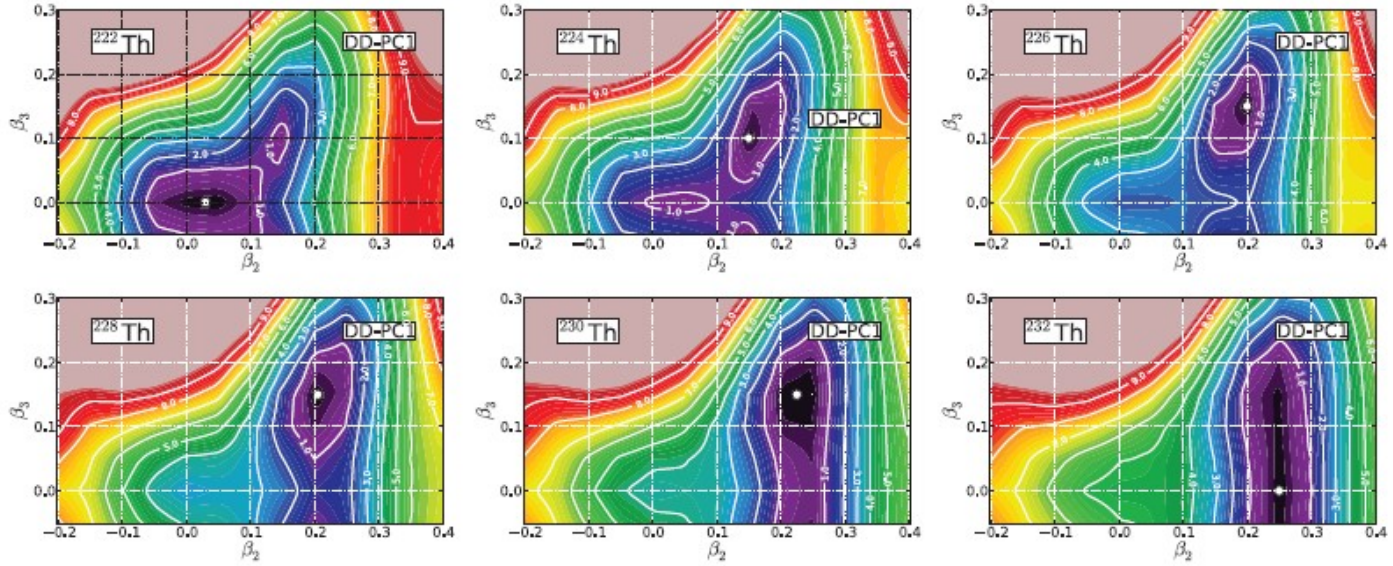

FIG. 1. (Color online) Axially symmetric energy surfaces of the isotopes $^{222-232}$Th in the (β_2, β_3) plane, calculated using the self-consistent RHB model with the microscopic functional DD-PC1. The contours join points on the surface with the same energy (in MeV), and the color scale varies in steps of 0.2 MeV. The energy difference between neighboring contours is 1 MeV. Note that energy surfaces are symmetric with respect to the $\beta_3 = 0$ axis. Open circles denote the absolute energy minima.

PHYSICAL REVIEW C **79**, 054301 (2009)

Microscopic analysis of nuclear quantum phase transitions in the $N \approx 90$ region

Z. P. Li,* T. Nikšić, and D. Vretenar

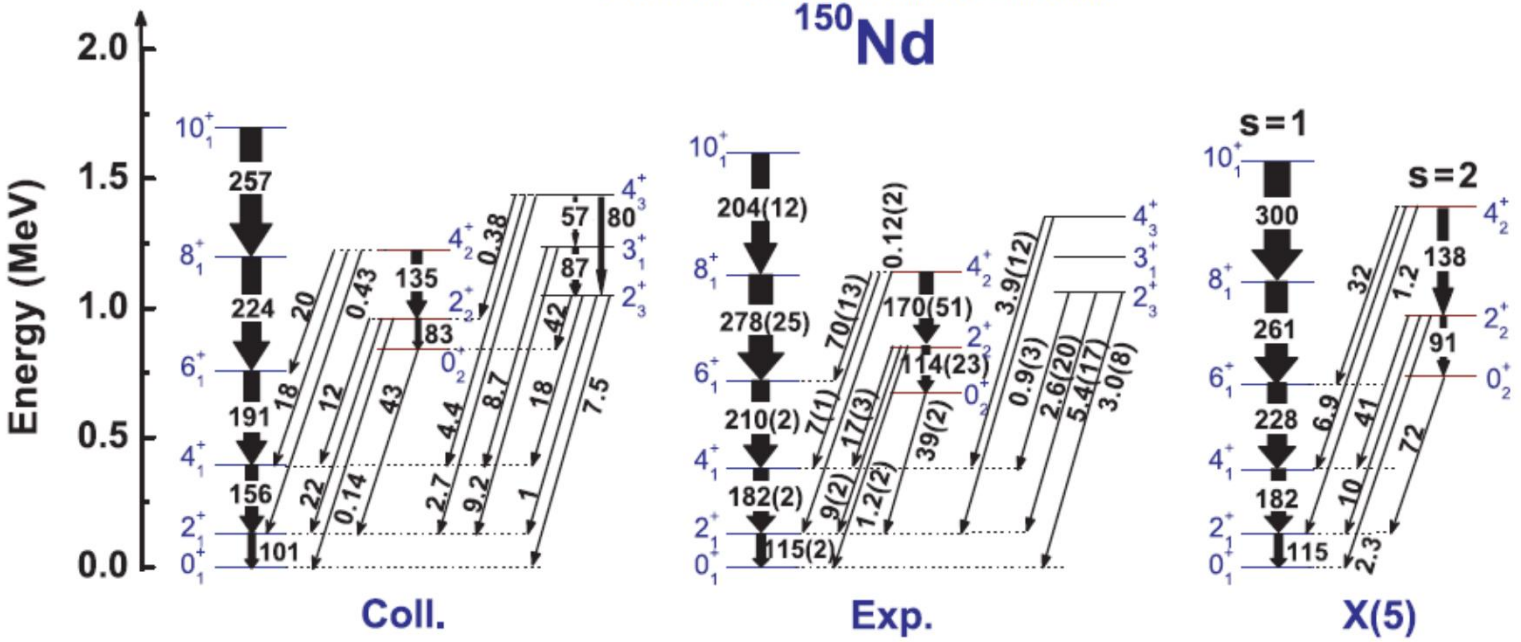

FIG. 6. (Color online) The spectrum of ^{150}Nd calculated with the PC-F1 relativistic density functional (left) compared with the data [34] (middle) and the X(5)-symmetry predictions (right) for the excitation energies and intraband and interband $B(E2)$ values (in W.u.) of the ground-state ($s = 1$) and β_1 ($s = 2$) bands. The theoretical spectra are normalized to the experimental energy of the state 2_1^+, and the X(5) transition strengths are normalized to the experimental $B(E2; 2_1^+ \rightarrow 0_1^+)$.

For the moments of inertia of the collective Hamiltonian we have multiplied the Inglis-Belyaev values Eq. (7) with a common factor determined in such a way that the calculated energy of the 2_1^+ state coincides with the experimental value.

GCM replaced by a 5D collective Hamiltonian

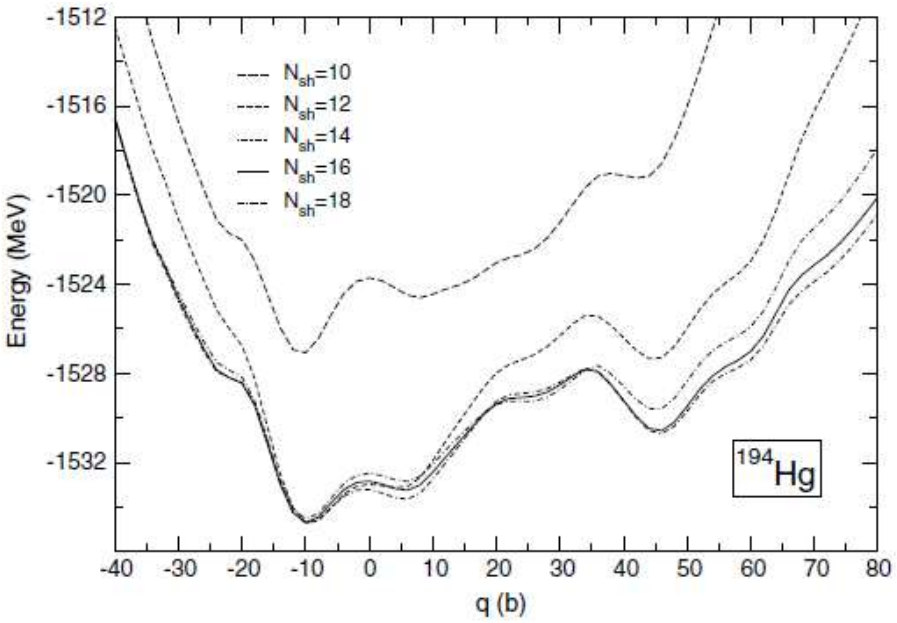

FIG. 1. The binding energy curves for ^{194}Hg, as functions of the moment, calculated by ex spinors in 10, 12, 14, 16, and

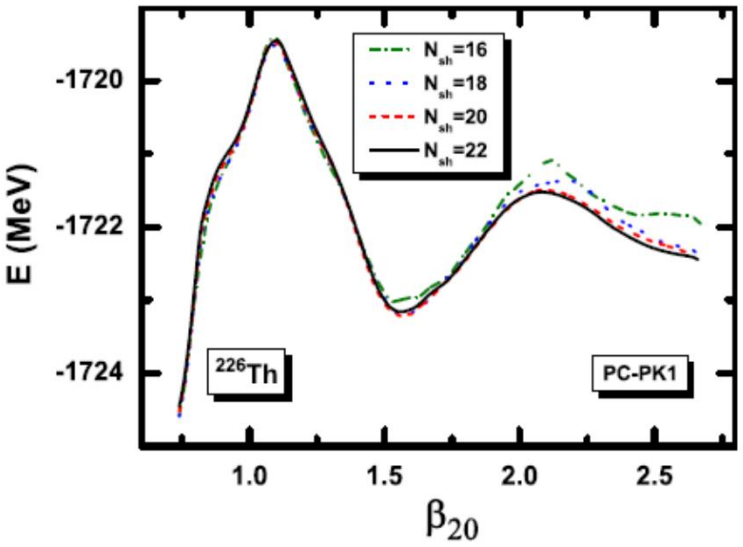

FIG. 2. (Color online) The axially symmetric energy curve of ^{226}Th computed with the MDC-RMF model, using the functional PC-PK1. Results obtained with different truncations of the ADHO basis, i.e., with $N_f = 16$, 18, 20, and 22 shells are plotted by the dash-dotted, dotted, dashed, and solid curves, respectively.

Axial basis
Choice of the oscillator length?
Optimization?

Systematic study of infrared energy corrections in truncated oscillator spaces

Alexander Arzhanov,[1,2] Tomás R. Rodríguez,[3] and Gabriel Martínez-Pinedo[1,2]

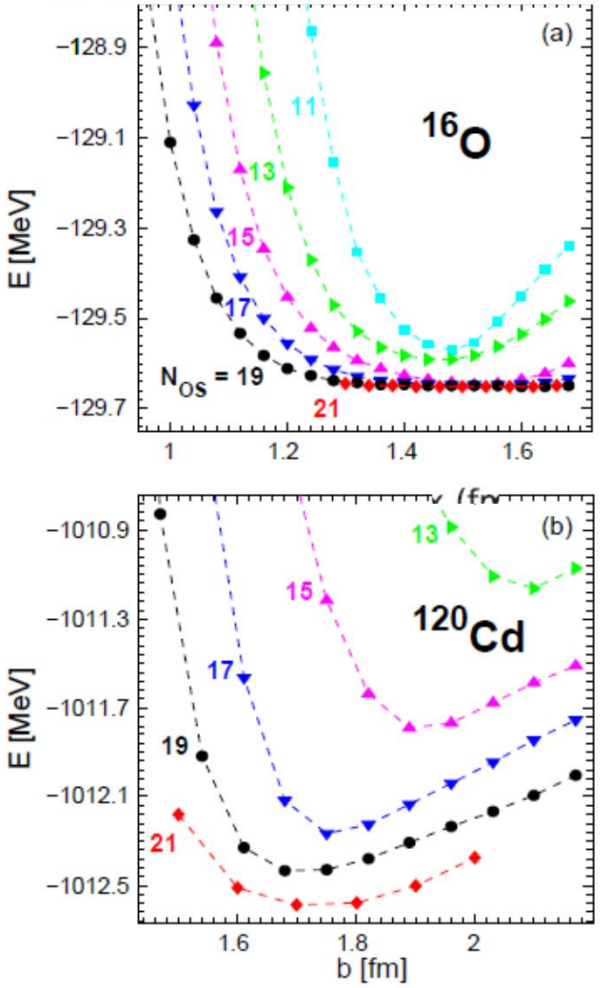

FIG. 2. (color online) HFB energies calculated in different bases $N_{OS} = 11,...,21$ (see labels at each curve) as a function of oscillator length b for (a) ^{16}O, and (b) ^{120}Cd.

The numerical technique: discretization on a 3-dimensional mesh

Lagrange derivatives (J. Phys. A 19 2041 (1986))

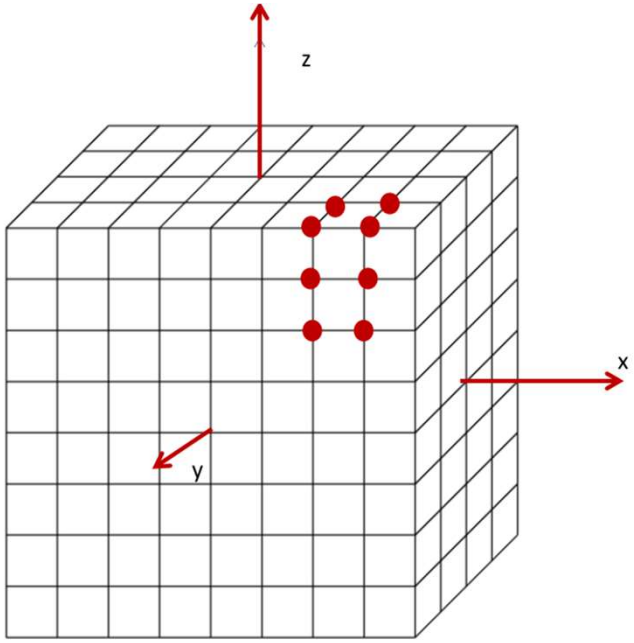

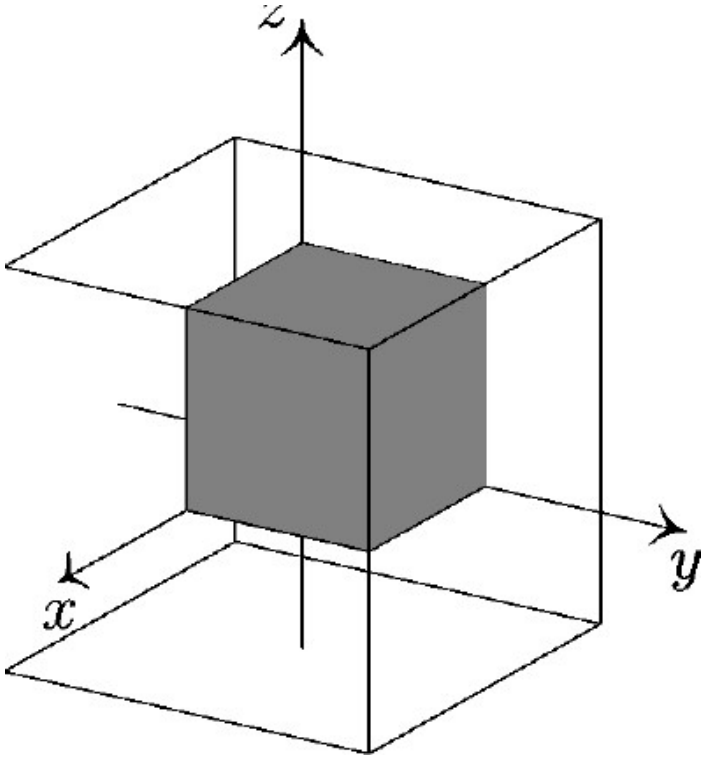

Why octupoles?

performed using accelerated beams of heavy, radioactive ions. Our data on ^{220}Rn and ^{224}Ra show clear evidence for stronger octupole deformation in the latter. The results enable discrimination between differing theoretical approaches to octupole correlations, and help to constrain suitable candidates for experimental studies of atomic electric-dipole moments that might reveal extensions to the standard model.

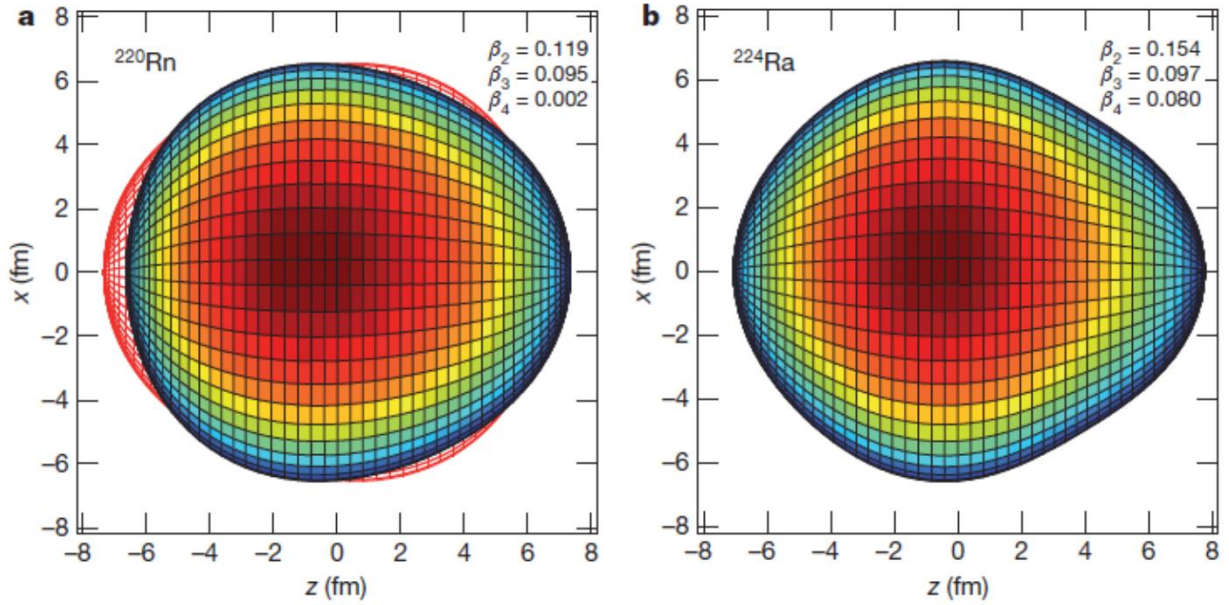

Figure 4 | Graphical representation of the shapes of ^{220}Rn and ^{224}Ra. **a**, ^{220}Rn; **b**, ^{224}Ra. Panel **a** depicts vibrational motion about symmetry between the surface shown and the red outline, whereas **b** depicts static deformation in the intrinsic frame. Theoretical values of β_4 are taken from ref. 10. The colour scale, blue to red, represents the y-values of the surface. The nuclear shape does not change under rotation about the z axis.

Gaffney, Butler et al.

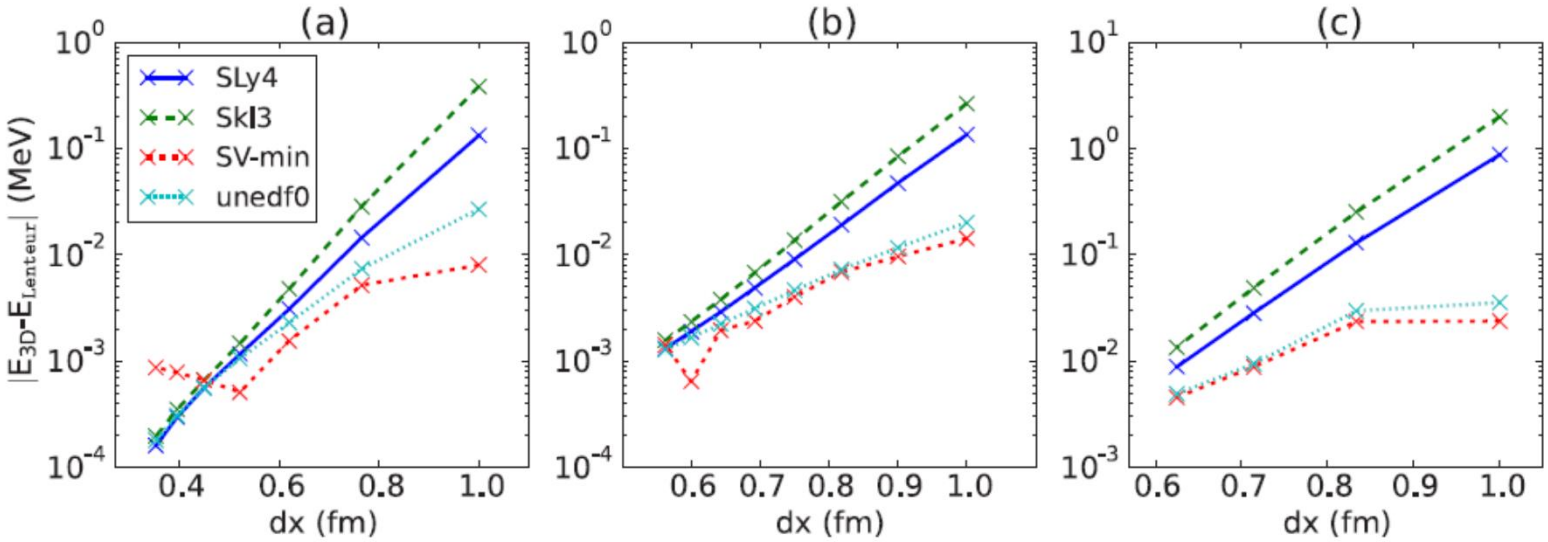

FIG. 5. (Color online) Differences between the total energy calculated with our 3D code and that calculated with the spherical code LENTEUR for ^{40}Ca (a), ^{132}Sn (b), and ^{208}Pb (c), as a function of the mesh distance dx. Results are plotted for a representative set of Skyrme parametrizations, without pairing. Results for SLy5, T22, and T65 are not shown but are indistinguishable from the SLy4 results at the scale of this graph.

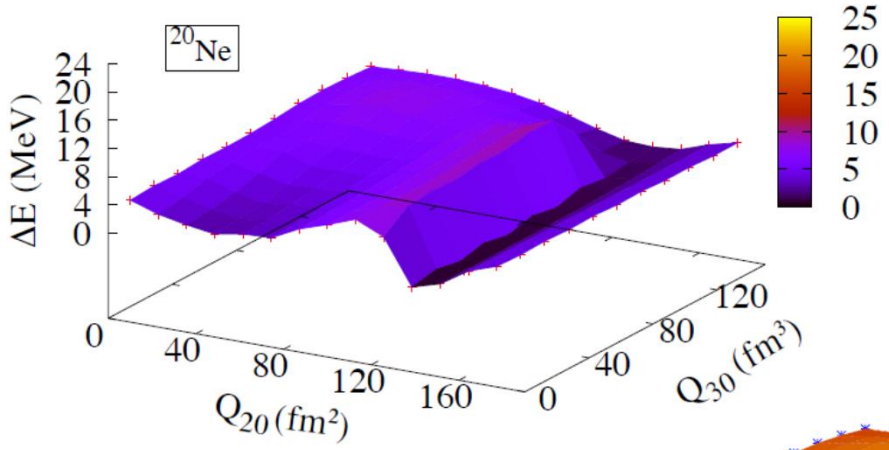

- no pairing, only HF
- SLy5 Skyrme interaction

- Octupole deformed minimum after PP+ +AMP projection

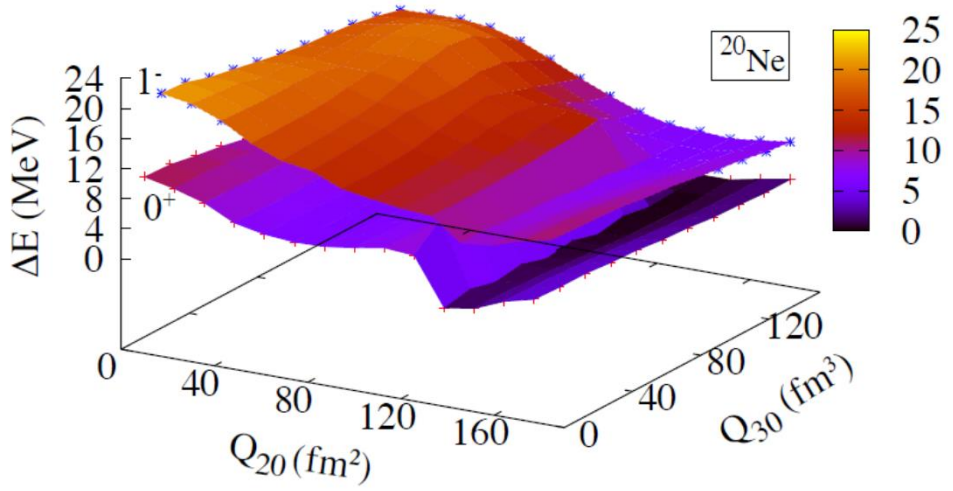

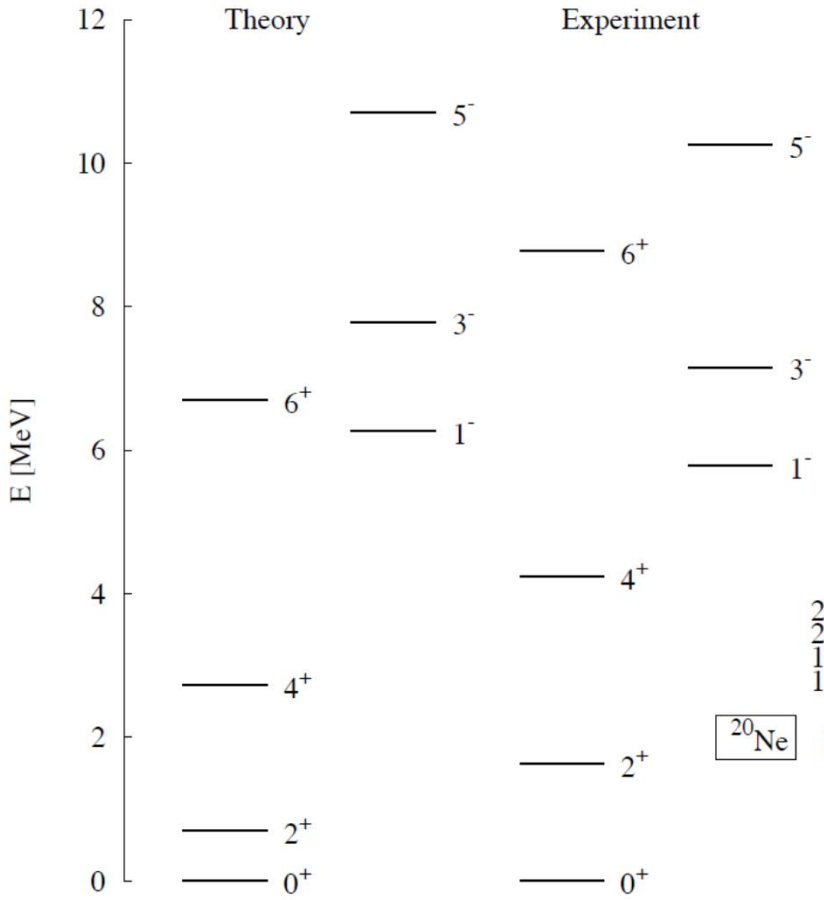

- Configuration mixing after parity and J-projection
- Q_{20} and Q_{30} degrees of freedom

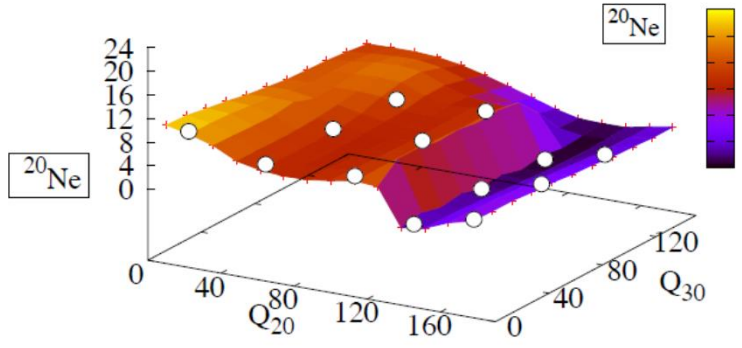

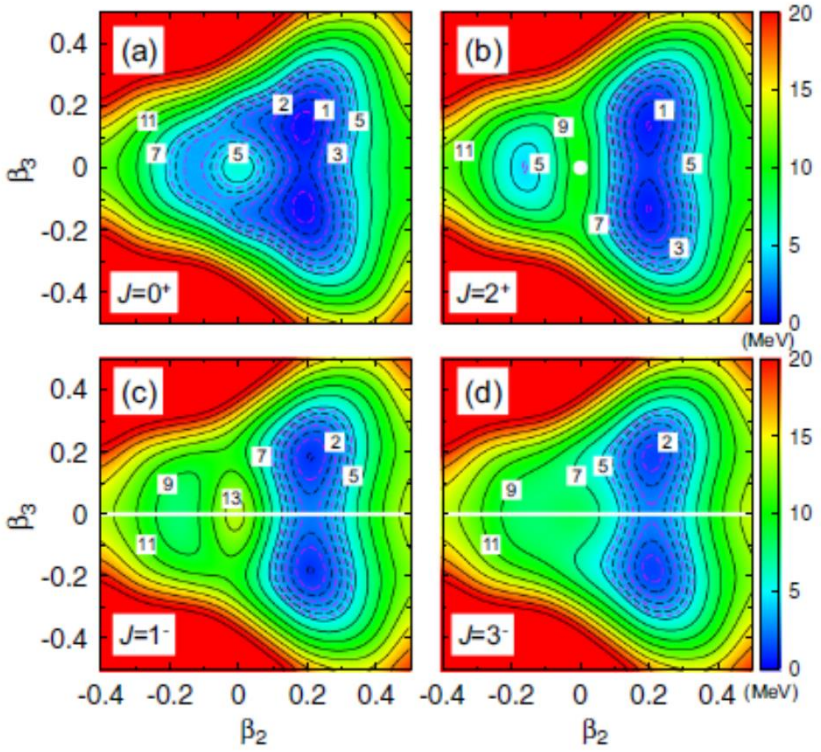

FIG. 2. Particle number, parity, and angular momentum PES in the (β_2,β_3) plane normalized to the energy of the minimum of the 0^+-PES (-1185.600 MeV with eleven HO shells). Contour lines are separated by 0.5 MeV (dashed lines) and 2.0 MeV (full lines) respectively.

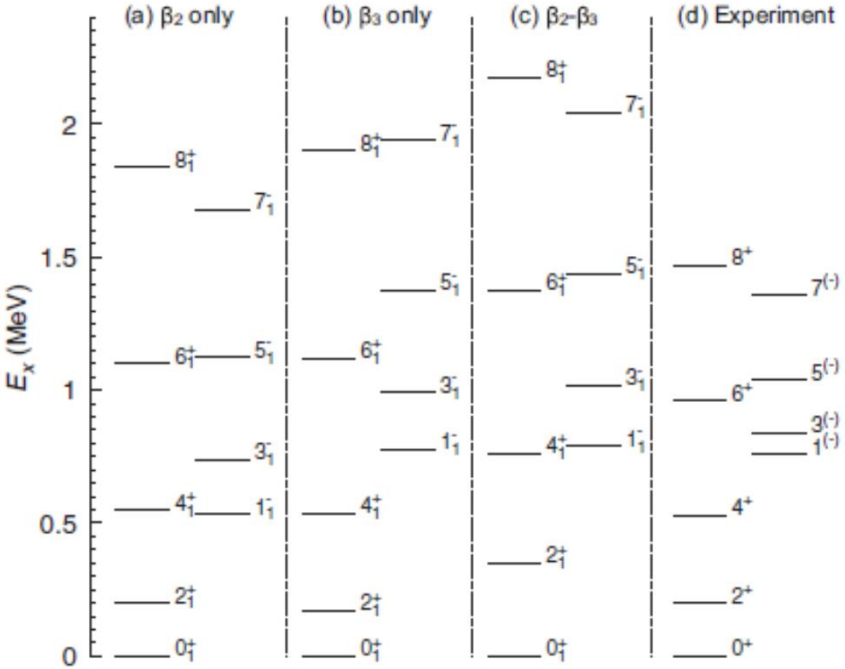

FIG. 3. Spectra (first two bands) obtained from SCCM calculations with (a) β_2, (b) β_3, and (c) $\beta_2-\beta_3$ as generating coordinates for ^{144}Ba. Experimental data (d) are taken from Ref. [36].

^{64}Ge, SLy4, HFB and projection on N, Z and J

Min of Q_2 for each Q_3 (nearly constant)

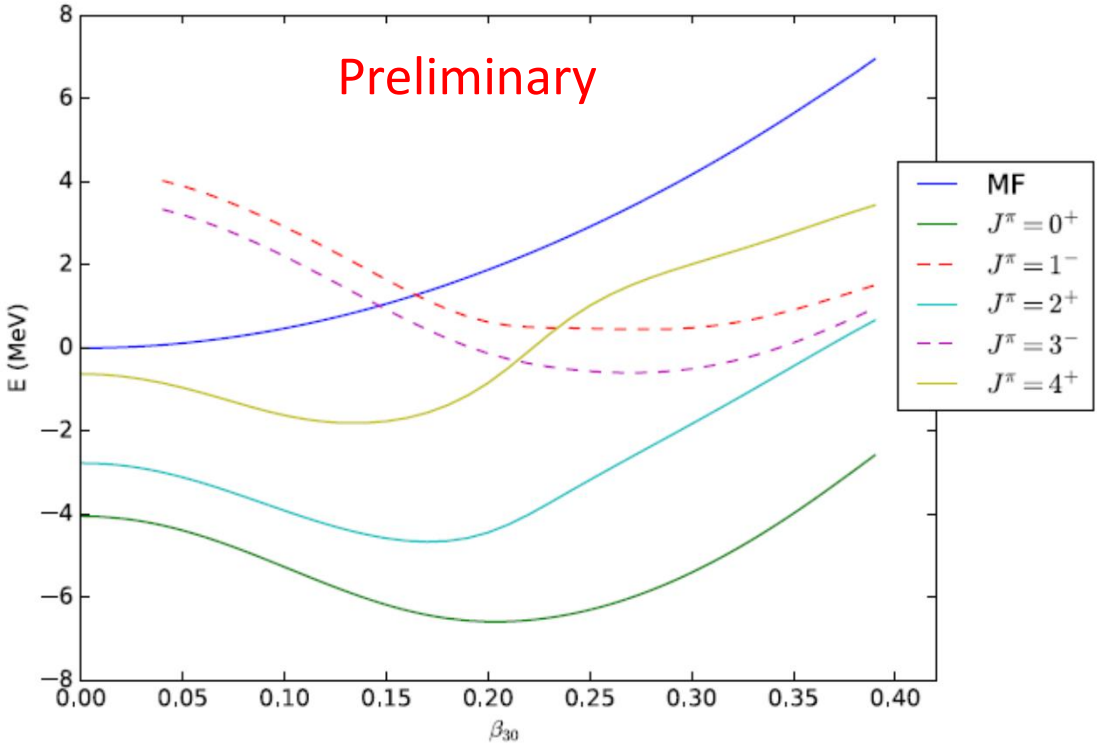

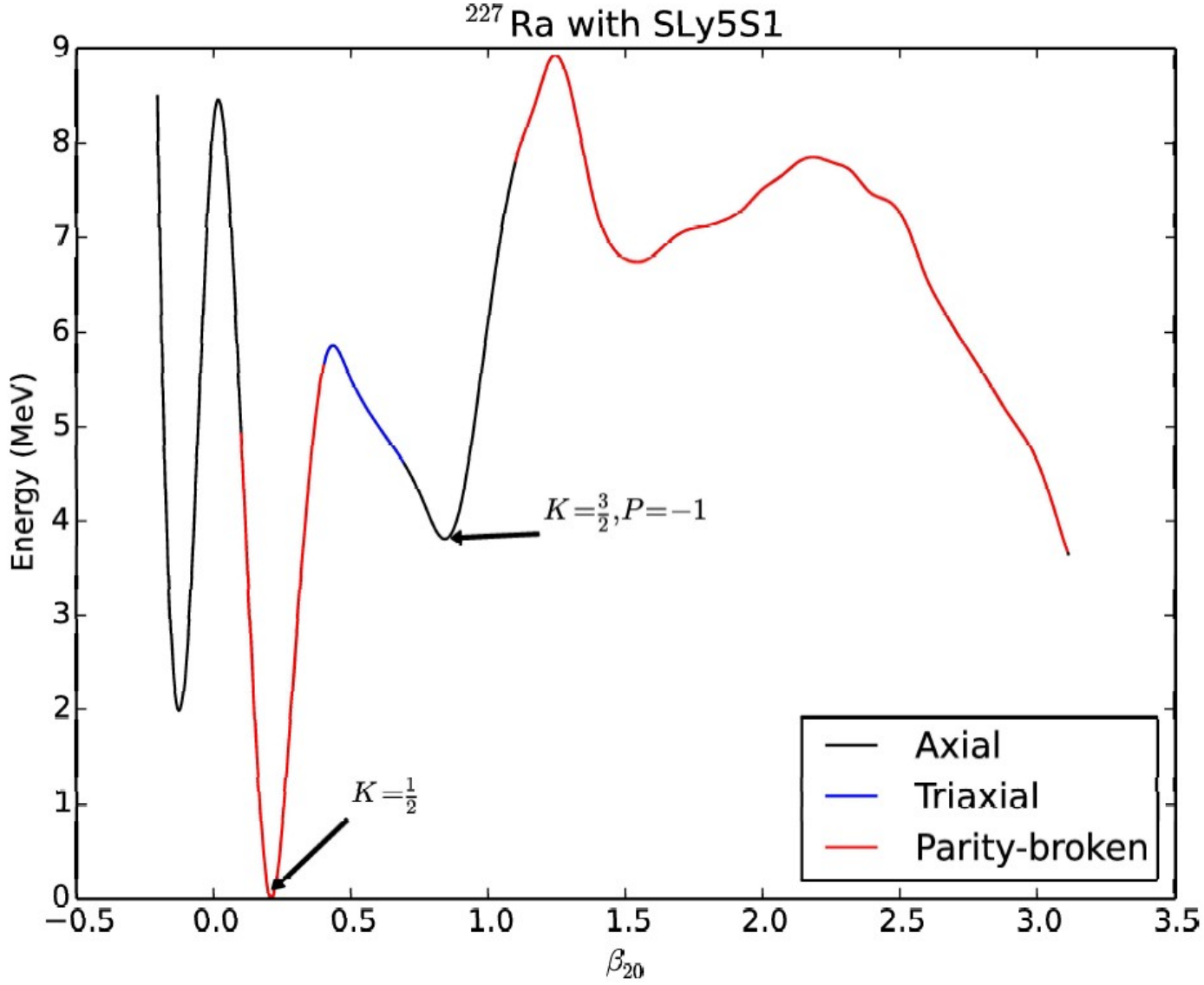
^{227}Ra with SLy5S1
Energy (MeV)
β_{20}
$K=\frac{3}{2},P=-1$
$K=\frac{1}{2}$
Axial
Triaxial
Parity-broken

^{180}Hg Calculation for SLy5s1